Unbalanced Control Strategy for A Thyristor-Controlled *LC*-Coupling Hybrid Active Power Filter in Three-Phase Three-Wire Systems

Lei Wang, Chi-Seng Lam, *Senior Member, IEEE*, and Man-Chung Wong, *Senior Member, IEEE*

***Abstract*—This paper proposes a control strategy for a three-phase three-wire thyristor-controlled *LC*-coupling hybrid active power filter (TCLC-HAPF), which can balance active power and compensate reactive power and harmonic currents under unbalanced loading. Compared with TCLC-HAPF with conventional control strategy, active power filters and hybrid active power filters which either fail to perform satisfactory compensation or require high-rating active inverter part for unbalanced compensation, a control strategy was proposed for TCLC-HAPF to operate with a small rating active inverter part for a variety of loads with satisfactory performance. The control idea is to provide different firing angles for each phase of the thyristor-controlled *LC*-coupling part (TCLC) to balance active power and compensate reactive power, while the active inverter part aims to compensate harmonic currents. First, the required different TCLC impedances are deduced. Then, independent firing angles referenced to the phase angle of voltage across TCLC are calculated. After angle transformations, final firing angles referenced to phase angle of load voltages are obtained. In this paper, a novel controller for TCLC-HAPF under unbalanced loading is proposed. Simulation and experimental results are provided to verify the effectiveness of the proposed controller in comparison with a state-of-the-art controller.**

***Index Terms*—Active power, current harmonics, hybrid active power filter (HAPF), reactive power, thyristor-controlled *LC*-coupling hybrid active power filter (TCLC-HAPF), unbalanced compensation.**

I. Introduction

UNDER practical conditions, when unbalanced nonlinear inductive loads are connected to the three-phase utility distribution system, a number of current quality problems, such as low power factor (PF), harmonic pollution, and unbalanced currents will rise. If compensation is not provided to the distribution power system, it will cause a series of undesirable consequences, such as additional heating and loss in the stator windings, damage on the overloaded phase power cable, reduction of transmission capability, increase in transmission loss, etc [1]–[4]. Implementation of power filters is one of the solutions for power quality problems. In the early days, thyristor-based static var compensators (SVCs) are used. It can inject or absorb reactive power according to different loading situations [1]–[4]. However, SVCs have many inherent problems including resonance problem, slow response, lack of harmonic compensation ability, and self-harmonic generation. Later on, the remarkably progressive concept of active power filters (APFs) was first proposed in 1976 for dynamically compensating reactive power and current harmonics problems [5]–[13]. However, APFs require high dc-link voltage levels ($V_{\rm dc} > \sqrt{2} \cdot V_{L-L}$) to perform compensation, which drives up their initial and operational costs. Afterward, in order to reduce the cost of APFs, an *LC*-coupling hybrid active power filter (HAPF) with low dc-link operational voltage was proposed by Akagi and Srianthumrong [14] in 2003. Unfortunately, HAPF has a narrow compensation range, which may require a high dc-link operation voltage when it is operating outside its compensation range, thus losing its low inverter rating characteristic [14]–[19]. Many control techniques have been proposed to improve the performance of the APFs and HAPFs and solve the unbalanced problems [5]–[21]. The different current quality compensators and their unbalanced control methods are summarized in Table I, and also compared in the following.

Akagi *et al.* [5] first proposed instantaneous *pq* control method in order to eliminate the reactive power, harmonic power, and unbalanced power of the loading instantaneously. In order to adapt instantaneous *pq* control method under different voltage conditions (distorted, unbalanced, etc), many other control techniques were further developed, such as dq control method [6], [7], [14]–[17], *pqr* control method [8], [9], Lyapunov function-based control method [18], etc. However, those instantaneous power control methods [5]–[9], [14]–[18] are dedicated to inverter/converter-based structures and their corresponding performances are highly dependent on the computation speed and the switching frequency of the digital controllers and the switching devices. On the other hand, another popular control method for APFs and HAPFs is to balance the system by compensating the negative- and zero-sequence current components under unbalanced loading situation, as the oscillating power/voltages/currents can be analytically expressed as positive-, negative-, and zero-sequence components ($+$, $-$, and 0 sequences) [10]. The major drawback of this control method is that the sequence components introduced by harmonics are

Manuscript received April 26, 2015; revised July 4, 2015, August 31, 2015, and December 23, 2015; accepted April 11, 2016. Date of publication April 20, 2016; date of current version November 11, 2016. This work was supported in part by the Macau Science and Technology Development Fund (FDCT) (FDCT 109/2013/A3) and in part by the Research Committee of the University of Macau (MRG012/WMC/2015/FST, MYRG2015-00030-AMSV). Recommended for publication by Associate Editor B. Singh. *(Corresponding author: Chi-Seng Lam.)*

L. Wang is with the Department of Electrical and Computer Engineering, Faculty of Science and Technology, University of Macau, Macau 999078, China.

C.-S. Lam is with the State Key Laboratory of Analog and Mixed Signal VLSI, University of Macau, Macau 999078, China (e-mail: cslam@umac.mo; c.s.lam@ieee.org).

M. C. Wong is with the Department of Electrical and Computer Engineering, Faculty of Science and Technology, and also with the State Key Laboratory of Analog and Mixed Signal VLSI, University of Macau, Macau 999078, China.

Color versions of one or more of the figures in this paper are available online at http://ieeexplore.ieee.org.

Digital Object Identifier 10.1109/TPEL.2016.2555330

TABLE I
CHARACTERISTICS OF DIFFERENT COMPENSATORS AND THEIR UNBALANCED CONTROL METHODS

	SVCs [1]-[4]	APFs [5]-[13],[20]-[21]	HAPFs [14]-[19]	TCLC-HAPF [22]
Year	1960s	1976	2003	2014
Resonance problem	Yes	No	No	No
Rating of active inverter part	--	High	Low	Low
Harmonic compensation	Poor	Good	Medium	Good
Dynamic Reactive power compensation	Good	Very good	Good	Very good
Compensation range	Wide	Wide	Narrow	Wide
Unbalanced compensation methods	+, - and 0 sequence methods [1]-[4]	1) Instantaneous power methods [5]-[9] 2) +, - and 0 sequence methods [10]-[13] 3) Power analysis method [20]-[21]	1) Instantaneous power methods [14]-[18] 2) +, - and 0 sequence methods [19]	Lack of study (Proposed in this paper)

*Notes: The shaded areas mean unfavorable characteristic.

not taken into consideration. To solve this problem, the authors in [11]–[13] and [19] combine the above instantaneous control methods with the $+$, $-$, and 0 sequence control method, but the computation steps increase a lot, thus significantly increasing the control complexity. Recently, Czarnecki *et al.* [20], [21] proposed a power analysis control method based on the theory of currents' physical component to compensate the reactive power in unbalanced three-phase four-wire system. However, after this power analysis method compensation, the active power remains unbalanced, which means the unbalance power cannot be completely eliminated.

With all the above control methods, both APFs [5]–[13], [20], [21] and HAPFs [14]–[18] can effectively compensate the reactive power and harmonic currents under unbalanced loading compensation. However, both APFs and HAPFs probably require high active inverter rating (high initial cost and switching loss) to perform unbalanced current compensation due to the inductive coupling structures of APFs and the narrow compensation range limitations of HAPFs. In 2014, Rahmani *et al.* [22] proposed the structure of a thyristor-controlled *LC*-coupling hybrid active power filter (TCLC-HAPF) which can operate with a small rating active inverter part for reactive power and harmonic current compensation in comparison to the conventional solutions [5]–[21]. To control TCLC-HAPF, a state-of-the-art control method is proposed in [22] to reduce the steady-state error of the TCLC part and improve the performance of current tracking and voltage regulation of the active inverter part. However, the control method proposed in [22] was designed based on the assumption of balanced loading condition. If this control method is applied to TCLC-HAPF for unbalanced loading compensation, it either fails to perform acceptable current quality compensation or requires a high-rating active inverter part for compensation, which results in increasing the system initial cost, switching loss, and switching noise. Therefore, this paper proposes a hybrid unbalanced control method for the TCLC-HAPF, which can balance source side active power and compensate the reactive power and harmonic currents with small rating active inverter part. The control idea is to generate different firing angles to each phase of the TCLC in order to compensate reactive power and balance active power, and the active inverter part aims to compensate the harmonic currents. As a result, the voltage rating of the active inverter part can be small, and, consequently, the system initial cost and switching noise can be significantly reduced. Moreover, the TCLC-HAPF can still maintain a wide compensation range with satisfactory performance comparable to the conventional solutions [5]–[21]. The proposed unbalanced controlled TCLC-HAPF is a cost-effective solution to compensate reactive power, harmonic pollution, and unbalanced currents in distribution system, especially for the medium voltage-level distribution system. In addition, given that most of the loads in the distribution power systems are inductive, the following analysis and discussion will only focus on inductive loads [23].

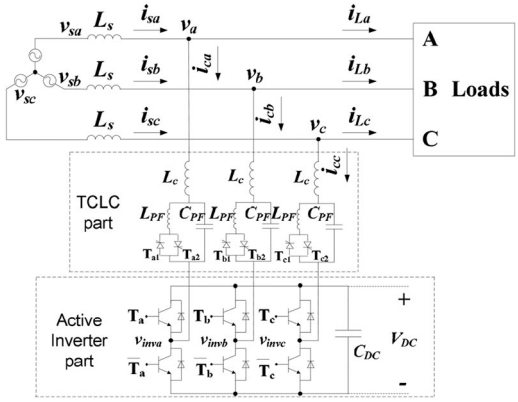

Fig. 1. Circuit configuration of a three-phase three-wire TCLC-HAPF.

In this paper, a brief introduction of research background and motivation is covered in Section I. In Section II, the circuit configuration of the TCLC-HAPF is presented and discussed. In Section III, the hybrid controller for the TCLC-HAPF under unbalanced loading is proposed and explained. Afterward, simulation and experimental results are given to verify the effectiveness of the proposed unbalanced control strategy for the TCLC-HAPF in comparison with the state-of-the-art control method [22] in Section IV. Finally, conclusion is drawn in Section V.

II. CIRCUIT CONFIGURATION OF A THREE-PHASE THREE-WIRE TCLC-HAPF

The circuit configuration of a three-phase three-wire TCLC-HAPF is given in Fig. 1, where the subscript "x" denotes phase $x = a, b, c$. v_{sx}, v_x, and $v_{\mathrm{inv}x}$ are the system voltage, load voltage, and inverter output voltage, respectively; L_s is the system inductance; i_{sx}, i_{Lx}, and i_{cx} are the source, load, and compensated currents, respectively. C_{DC} and V_{DC} are dc-link capacitor and dc-link voltage; L_c is the coupling inductor; L_{PF} and C_{PF} are the TCLC part inductor and capacitor.

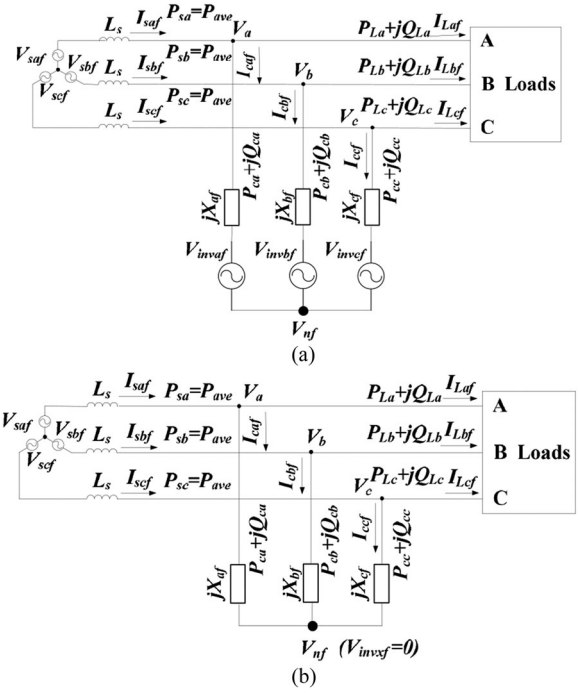

Fig. 2. Equivalent fundamental circuit models of the TCLC-HAPF when: (a) $V_{\mathrm{inv}x} \neq 0$ and (b) $V_{\mathrm{inv}xf} = 0$.

In this topology, the TCLC part and the active inverter part can complement each other's disadvantages. As the TCLC part offers the reactive power compensation range and provides a large voltage drop between load voltage and inverter voltage, the voltage rating of the active inverter part can be significantly reduced. On the other hand, the active inverter part can solve the inherent problems of using TCLC alone, such as inrush currents, resonance problem, noise of thyristors turning on/off, mistuning of firing angles, and low-harmonic compensation ability. Based on the circuit configuration as shown in Fig. 1, the unbalanced control strategy for the TCLC-HAPF will be proposed in next section.

III. Proposed Unbalanced Control Strategy for TCLC-HAPF

The purposes of the proposed unbalanced control strategy can be described as follows: the TCLC part is controlled to balance active power and compensate reactive power, while the active inverter part aims to compensate harmonic currents. The equivalent fundamental circuit models of the TCLC-HAPF for power analysis are illustrated in Fig. 2, where the subscripts "f" denotes the fundamental frequency component. In this paper, V_{sxf} and V_{xf} are assumed to be pure sinusoidal without harmonic components ($V_x = V_{sxf} = V_{xf}$) for simplicity.

Fig. 2 is used to calculate the required impedances and the corresponding firing angles for each phase of the TCLC part in order to balance and compensate active and reactive power. In Fig. 2(a), the active inverter can be treated as a controlled voltage source, and the required fundamental inverter voltage ($V_{\mathrm{inv}xf}$) depends on the TCLC impedance [24]–[26]. If the TCLC impedance is perfectly matched with the load impedance, then the required $V_{\mathrm{inv}xf}$ can be equal to zero. In this paper, it is assumed that the TCLC is controlled to be perfectly matched with the loading to simplify the following analysis; thus, $V_{\mathrm{inv}xf} = 0$, then the required TCLC impedance can be calculated based on Fig. 2(b). In the following, the proposed hybrid control strategy for the TCLC-HAPF under unbalanced loading compensation will be presented and explained in three sections: Section III-A: TCLC part control strategy, which is based on the fundamental model in Fig. 2(b), Section III-B: Active inverter part control strategy, and Section III-C: The overall hybrid controller for TCLC-HAPF.

A. TCLC Part Control Strategy

From the mathematical analysis as shown in *Appendix A*, it can be clearly illustrated that the three-phase source active power can become balanced once the reactive power is compensated. With this idea, the control target of the TCLC part is dedicated to balance and compensate the fundamental active and reactive power via the calculated required firing angles in this paper. The firing angles are determined by the required TCLC impedances (X_{af}, X_{bf}, and X_{cf}) for compensation which can be deduced by Ohm's law. Referring to Fig. 2(b), in order to obtain the required TCLC impedances (X_{af}, X_{bf}, and X_{cf}) for each phase, the virtual common point (V_{nf}) is calculated first. Then, the TCLC impedance of each phase can be obtained by $X_{xf} = (V_x - V_{nf})/I_{cxf}$, $x = a, b, c$, where I_{cxf} is expressed in terms of each phase load power and V_x. After that three independent firing angles $\alpha_{0,x}$ referenced to the phase angle of the voltage drop ($V_x - V_{nf}$) across the TCLC can be obtained. Since the control of the firing angles of the TCLC usually reference to the phase angle of the load voltage V_x of each phase, an angle transformation process is required and also proposed in this paper.

Based on the above discussion, there are three steps to find the final firing angles α_x for controlling the TCLC, namely: 1) Calculation of V_{nf}, 2) obtain the impedances of X_{af}, X_{bf}, and X_{cf}, and 3) find the final firing angles α_x for each phase referenced to the phase angle of V_x. In addition, a case study is provided in *Appendix B* to verify the proposed TCLC control method.

1) Calculation of V_{nf}: Based on Fig. 2(b), the sum of the compensating currents can be obtained by applying the Kirchhoff's circuit laws as

$$\vec{I}_{caf} + \vec{I}_{cbf} + \vec{I}_{ccf} = \frac{\vec{V}_a - \vec{V}_{nf}}{jX_{af}} + \frac{\vec{V}_b - \vec{V}_{nf}}{jX_{bf}} + \frac{\vec{V}_c - \vec{V}_{nf}}{jX_{cf}} = 0 \tag{1}$$

where $\vec{I}_{caf}$, $\vec{I}_{cbf}$, and $\vec{I}_{ccf}$ are vector forms of fundamental compensating currents. $\vec{V}_a$, $\vec{V}_b$, and $\vec{V}_c$ are the vector forms of load voltages. From (1), $\vec{V}_{nf}$ can be obtained as

$$\vec{V}_{nf} = \frac{X_{bf} \cdot X_{cf}}{X_{af}X_{bf} + X_{bf}X_{cf} + X_{cf}X_{af}} \cdot \vec{V}_a + \frac{X_{cf} \cdot X_{af}}{X_{af}X_{bf} + X_{bf}X_{cf} + X_{cf}X_{af}} \cdot \vec{V}_b$$

$$+\frac{X_{af}\cdot X_{bf}}{X_{af}X_{bf}+X_{bf}X_{cf}+X_{cf}X_{af}}\cdot\vec{V}_c. \tag{2}$$

With the expression of $\vec{V}_{nf}$, the TCLC impedances can be obtained by Ohm's law as discussed in the next part.

2) Obtain the Impedance of X_{af}, X_{bf}, and X_{cf}: From (1) and (2), the relationship among the phase compensating currents $\vec{I}_{cxf}$, load voltages $\vec{V}_x$, and coupling impedances X_{xf} can be expressed as

$$\begin{bmatrix}\vec{I}_{caf}\\ \vec{I}_{cbf}\\ \vec{I}_{ccf}\end{bmatrix}= \begin{bmatrix}(jX_{af})^{-1} & 0 & 0\\ 0 & (jX_{bf})^{-1} & 0\\ 0 & 0 & (jX_{cf})^{-1}\end{bmatrix}\cdot\begin{bmatrix}\vec{V}_a-\vec{V}_{nf}\\ \vec{V}_b-\vec{V}_{nf}\\ \vec{V}_c-\vec{V}_{nf}\end{bmatrix}$$
$$=\begin{bmatrix}-j\left(\frac{X_{bf}+X_{cf}}{m}\right) & j\frac{X_{cf}}{m} & j\frac{X_{bf}}{m}\\ j\frac{X_{cf}}{m} & -j\left(\frac{X_{af}+X_{cf}}{m}\right) & j\frac{X_{af}}{m}\\ j\frac{X_{bf}}{m} & j\frac{X_{af}}{m} & -j\left(\frac{X_{af}+X_{bf}}{m}\right)\end{bmatrix}\cdot\begin{bmatrix}\vec{V}_a\\ \vec{V}_b\\ \vec{V}_c\end{bmatrix} \tag{3}$$

where $\vec{V}_{nf}$ can be obtained from (2) and $m=X_{af}X_{bf}+X_{bf}X_{cf}+X_{cf}X_{af}$.

The compensating apparent power S_{cx} can be defined as $S_{cx}=P_{cx}+jQ_{cx}=\vec{V}_x\cdot\vec{I}^*_{cxf}$ where $\vec{I}^*_{cxf}$ is the conjugate of $\vec{I}_{cxf}$. Modifying S_{cx} equation, the expression of the phase compensating currents can be given as

$$\begin{bmatrix}\vec{I}_{caf}\\ \vec{I}_{cbf}\\ \vec{I}_{ccf}\end{bmatrix}=\begin{bmatrix}\left(\left(P_{ca}+jQ_{ca}\right)/\vec{V}_a\right)^*\\ \left(\left(P_{cb}+jQ_{cb}\right)/\vec{V}_b\right)^*\\ \left(\left(P_{cc}+jQ_{cc}\right)/\vec{V}_c\right)^*\end{bmatrix} \tag{4}$$

where the note "$*$" denotes the conjugate. $\vec{V}_a$ is set to be the reference phasor, so $\vec{V}_a=\bar{V}_x\angle 0^\circ$, $\vec{V}_b=\bar{V}_x\angle -120^\circ$, and $\vec{V}_c=\bar{V}_x\angle 120^\circ$, where $1\angle -120^\circ=-1/2-j\sqrt{3}/2$ and $1\angle 120^\circ=-1/2+j\sqrt{3}/2$, $\bar{V}_x$ is the root-mean-square (rms) value of load voltage which can be obtained in real time as $\bar{V}_x=\|v_L\|/\sqrt{3}=\sqrt{v_a^2+v_b^2+v_c^2}/\sqrt{3}$ [5]. Q_{cx} and P_{cx} are the compensating reactive power and active power. Theoretically, after compensation, the source reactive power should become zero and the source active power should all be equal to $(P_{La}+P_{Lb}+P_{Lc})/3$. Therefore, the reactive power and active power generated/absorbed by the TCLC part can be expressed as

$$Q_{cx}=-Q_{Lx}\quad\text{and}\quad P_{cx}=-\left(P_{Lx}-\frac{P_{La}+P_{Lb}+P_{Lc}}{3}\right) \tag{5}$$

where $x=a,\ b,\ c$, Q_{cx} and Q_{Lx} are the compensating and load reactive power, and P_{cx} and P_{Lx} are the compensating and load active power. Combining (1)–(5), the relationship between TCLC impedances and load power can be deduced as

$$\begin{bmatrix}X_{af}/m\\ X_{bf}/m\\ X_{cf}/m\end{bmatrix}=\begin{bmatrix}\left(Q_{ca}-Q_{cb}-Q_{cc}\right)/3\bar{V}_x^2\\ \left(Q_{cb}-Q_{ca}-Q_{cc}\right)/3\bar{V}_x^2\\ \left(Q_{cc}-Q_{cb}-Q_{ca}\right)/3\bar{V}_x^2\end{bmatrix} \tag{6}$$

where $m=X_{af}X_{bf}+X_{bf}X_{cf}+X_{cf}X_{af}$. Further simplifying (6), the coupling impedances X_{af}, X_{bf}, and X_{cf} can be obtained as

$$\begin{bmatrix}X_{af}\\ X_{bf}\\ X_{cf}\end{bmatrix}= \begin{bmatrix}\frac{3\cdot\bar{V}_x^2\cdot(Q_{Lc}-Q_{Lb}-Q_{La})^{-1}\cdot(Q_{Lb}-Q_{La}-Q_{Lc})^{-1}}{(Q_{Lc}-Q_{Lb}-Q_{La})^{-1}+(Q_{La}-Q_{Lb}-Q_{Lc})^{-1}+(Q_{Lb}-Q_{La}-Q_{Lc})^{-1}}\\ \frac{3\cdot\bar{V}_x^2\cdot(Q_{Lc}-Q_{Lb}-Q_{La})^{-1}\cdot(Q_{La}-Q_{Lb}-Q_{Lc})^{-1}}{(Q_{Lc}-Q_{Lb}-Q_{La})^{-1}+(Q_{La}-Q_{Lb}-Q_{Lc})^{-1}+(Q_{Lb}-Q_{La}-Q_{Lc})^{-1}}\\ \frac{3\cdot\bar{V}_x^2\cdot(Q_{La}-Q_{Lb}-Q_{Lc})^{-1}\cdot(Q_{Lb}-Q_{La}-Q_{Lc})^{-1}}{(Q_{Lc}-Q_{Lb}-Q_{La})^{-1}+(Q_{La}-Q_{Lb}-Q_{Lc})^{-1}+(Q_{Lb}-Q_{La}-Q_{Lc})^{-1}}\end{bmatrix}. \tag{7}$$

From (7), the TCLC impedances are expressed in terms of the phase load reactive power Q_{Lx} and rms voltage of phase load voltage $\bar{V}_x$. Then, the TCLC impedances are used to find the firing angles to control the TCLC part, which will be discussed in the following part.

3) Find the Final Firing Angles α_x Referenced to the Phase Angle of V_x: The impedance of the TCLC part can be considered as the X_{L_c} connected in series with the combination of $X_{C_{PF}}$ in parallel with a thyristor-controlled reactance (TCR) $X_{\mathrm{TCR}}(\alpha_{0,x})\left(=\frac{\pi}{2\pi-2\alpha_{0,x}+\sin 2\alpha_{0,x}}\cdot X_{L_{PF}}\right)$. Therefore, the expression of the TCLC impedances (X_{af}, X_{bf}, and X_{cf}) in terms of passive components and firing angles ($\alpha_{0,x}$) referenced to the phase angle of voltage across TCLC (V_x-V_{nf}) is shown as

$$\begin{bmatrix}X_{af}(\alpha_{0,a})\\ X_{bf}(\alpha_{0,b})\\ X_{cf}(\alpha_{0,c})\end{bmatrix}=\begin{bmatrix}\frac{\pi X_{L_{PF}}X_{C_{PF}}}{X_{C_{PF}}[2\pi-2\alpha_{0,a}+\sin(2\alpha_{0,a})]-\pi X_{L_{PF}}}+X_{L_c}\\ \frac{\pi X_{L_{PF}}X_{C_{PF}}}{X_{C_{PF}}[2\pi-2\alpha_{0,b}+\sin(2\alpha_{0,b})]-\pi X_{L_{PF}}}+X_{L_c}\\ \frac{\pi X_{L_{PF}}X_{C_{PF}}}{X_{C_{PF}}[2\pi-2\alpha_{0,c}+\sin(2\alpha_{0,c})]-\pi X_{L_{PF}}}+X_{L_c}\end{bmatrix} \tag{8}$$

where X_{L_c}, $X_{C_{PF}}$, and $X_{L_{PF}}$ are the impedances of the coupling inductor, the TCLC capacitor, and inductor, respectively. Equation (8) has a term of $-2\alpha_{0,x}+\sin(2\alpha_{0,x})$ and it does not have a closed-form solution. Therefore, a look-up table (LUT) has been implemented into the controller for performing simulations and experiments. Once the required coupling impedance $X_{xf}(\alpha_{0,x})$ is obtained from (7), the precalculated firing angle $\alpha_{0,x}$ can be extracted based on the LUT of (8). As the control of the firing angles of the TCLC is usually referenced to the phase angle of the load voltage V_x of each phase, an angle transformation process is required and proposed in the following.

Fig. 3 shows the angle relationship between the phase angle of the load voltage $\vec{V}_x$ and the phase angle of the voltage across TCLC (V_x-V_{nf}). From Fig. 3, there will be an angle difference

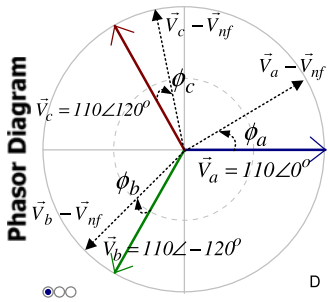

Fig. 3. Phasor diagram of load voltage $\vec{V}_x$ and the TCLC impedance voltage $\vec{V}_x - \vec{V}_{nf}$.

for each phase between that of the load voltage V_x and that of voltage across TCLC ($V_x - V_{nf}$), thus the above calculated firing angles $\alpha_{0,x}$ should have angle transformation if the control of the TCLC firing angles is referenced to the load voltage.

To keep the same impedance X_x in Section III-A2, an angle transformation process is required in order to obtain the final firing angle α_x referenced to the phase angle of the load voltage V_x. The final firing angles α_x can be obtained as

$$\begin{bmatrix} \alpha_a \\ \alpha_b \\ \alpha_c \end{bmatrix} = \begin{bmatrix} \alpha_{0,a} \\ \alpha_{0,b} \\ \alpha_{0,c} \end{bmatrix} - \begin{bmatrix} \phi_a \\ \phi_b \\ \phi_c \end{bmatrix} \tag{9}$$

where the phase angle ϕ_x is the phase angle of the voltage across TCLC, and ϕ_x can be calculated from the expression of $\overline{V}_{nf}$ in (2) as

$$\begin{bmatrix} \phi_a \\ \phi_b \\ \phi_c \end{bmatrix} = \begin{bmatrix} \tan^{-1}\left(\frac{X_{cf}-X_{bf}}{\sqrt{3}(X_{bf}+X_{cf})}\right) \\ \tan^{-1}\left(\frac{X_{af}-X_{cf}}{\sqrt{3}(X_{af}+X_{cf})}\right) \\ \tan^{-1}\left(\frac{X_{bf}-X_{af}}{\sqrt{3}(X_{bf}+X_{af})}\right) \end{bmatrix}_{\tan^{-1}\theta\in[-90^\circ,90^\circ]}. \tag{10}$$

Based on (7)–(10), the final firing angle α_x can be obtained in terms of phase load reactive power, load voltages, and the passive component values of the TCLC. The phase load reactive power can be obtained with the help of single phase *pq* theory [28] and low-pass filters.The trigger signals to control the TCLC part are generated by comparing the calculated α_x (9) with the phase angle of the load voltage θ_x, which is instantaneously measured by the phase-lock loop. The TCLC part has two back-to-back connected thyristors T_{x1} and T_{x2} for each phase, and they are triggered alternately in every half cycle. When $\theta_x > \alpha_x$, the gate pulse for thyristor T_{x1} can be generated. On the other hand, when $\theta_x < 180^\circ - \alpha_x$, the gate pulse for thyristor T_{x2} can be generated. In addition, the thyristors can turn on immediately when there is a trigger signal, while they can only be turned off when the inductor current goes to zero.

A case study is included in *Appendix B* to verify the above analysis in Sections III-A1–III-A3.

B. Active Inverter Part Control Strategy

If only the TCLC part control is used, the harmonic currents cannot be eliminated satisfactory. The purpose of the active inverter part is to instantaneously control the compensating current to track its reference, so that it can compensate the load harmonic currents and significantly improve the compensation ability and dynamic performance of the TCLC part. In the following, the active inverter part control can be discussed in three sections: Section III-B1: Instantaneous power compensation control, Section III-B2: the dc-link voltage control, and Section III-B3: current PWM control.

1) Instantaneous Power Compensation Control: As the generalized instantaneous power theory [5] is valid for unbalanced three-phase systems, it is chosen to calculate the reference compensating current $i_{cx\mathrm{ref}}$. The calculated $i_{cx\mathrm{ref}}$ contains the harmonics, reactive power, unbalanced power, and the dc-link voltage regulating components. By controlling the compensating current i_{cx} to its reference $i_{cx\mathrm{ref}}$, the active inverter part can compensate the load harmonic currents, improve the reactive power compensation ability and dynamic performance of the TCLC part, and also regulate the dc-link voltage to its reference value. The $i_{cx\mathrm{ref}}$ can be calculated through the well-known instantaneous *pq* theory [5] as

$$\begin{bmatrix} i_{ca\mathrm{ref}} \\ i_{cb\mathrm{ref}} \\ i_{cc\mathrm{ref}} \end{bmatrix} = \sqrt{\frac{2}{3}} \cdot \frac{1}{v_\alpha^2 + v_\beta^2} \begin{bmatrix} 1 & 0 \\ -1/2 & \sqrt{3}/2 \\ -1/2 & -\sqrt{3}/2 \end{bmatrix} \cdot \begin{bmatrix} v_\alpha & -v_\beta \\ v_\beta & v_\alpha \end{bmatrix} \cdot \begin{bmatrix} \tilde{p}_{\alpha\beta} + dc_p \\ q_{\alpha\beta} + dc_q \end{bmatrix} \tag{11}$$

where the dc_p and dc_q are the active and reactive components for dc-link voltage regulation, and the discussions of dc_p and dc_q are provided in the following Section III-B2. $p_{\alpha\beta}$ and $q_{\alpha\beta}$ is the instantaneous active and reactive power which include dc components $\bar{p}_{\alpha\beta}$ and $\bar{q}_{\alpha\beta}$, and ac components $\tilde{p}_{\alpha\beta}$ and $\tilde{q}_{\alpha\beta}$. $\bar{p}_{\alpha\beta}$ and $\bar{q}_{\alpha\beta}$ contain the fundamental active and reactive current components, respectively, while $\tilde{p}_{\alpha\beta}$ and $\tilde{q}_{\alpha\beta}$ contain harmonic currents and negative-sequence components. $\tilde{p}_{\alpha\beta}$ is obtained by passing $p_{\alpha\beta}$ through a high-pass filter. $p_{\alpha\beta}$ and $q_{\alpha\beta}$ can be obtained as

$$\begin{bmatrix} p_{\alpha\beta} \\ q_{\alpha\beta} \end{bmatrix} = \begin{bmatrix} v_\alpha & v_\beta \\ -v_\beta & v_\alpha \end{bmatrix} \cdot \begin{bmatrix} i_\alpha \\ i_\beta \end{bmatrix}. \tag{12}$$

In (11) and (12), the voltages (v_α and v_β) and currents (i_α and i_β) in $\alpha\beta$ plane are transformed from *abc* frames by

$$\begin{bmatrix} v_\alpha \\ v_\beta \end{bmatrix} = \begin{bmatrix} 1 & -1/2 & -1/2 \\ 0 & \sqrt{3}/2 & -\sqrt{3}/2 \end{bmatrix} \cdot \begin{bmatrix} v_a \\ v_b \\ v_c \end{bmatrix}$$

$$\begin{bmatrix} i_\alpha \\ i_\beta \end{bmatrix} = \begin{bmatrix} 1 & -1/2 & -1/2 \\ 0 & \sqrt{3}/2 & -\sqrt{3}/2 \end{bmatrix} \cdot \begin{bmatrix} i_{La} \\ i_{Lb} \\ i_{Lc} \end{bmatrix} \tag{13}$$

where v_x and i_{Lx} are load voltage and current signals.

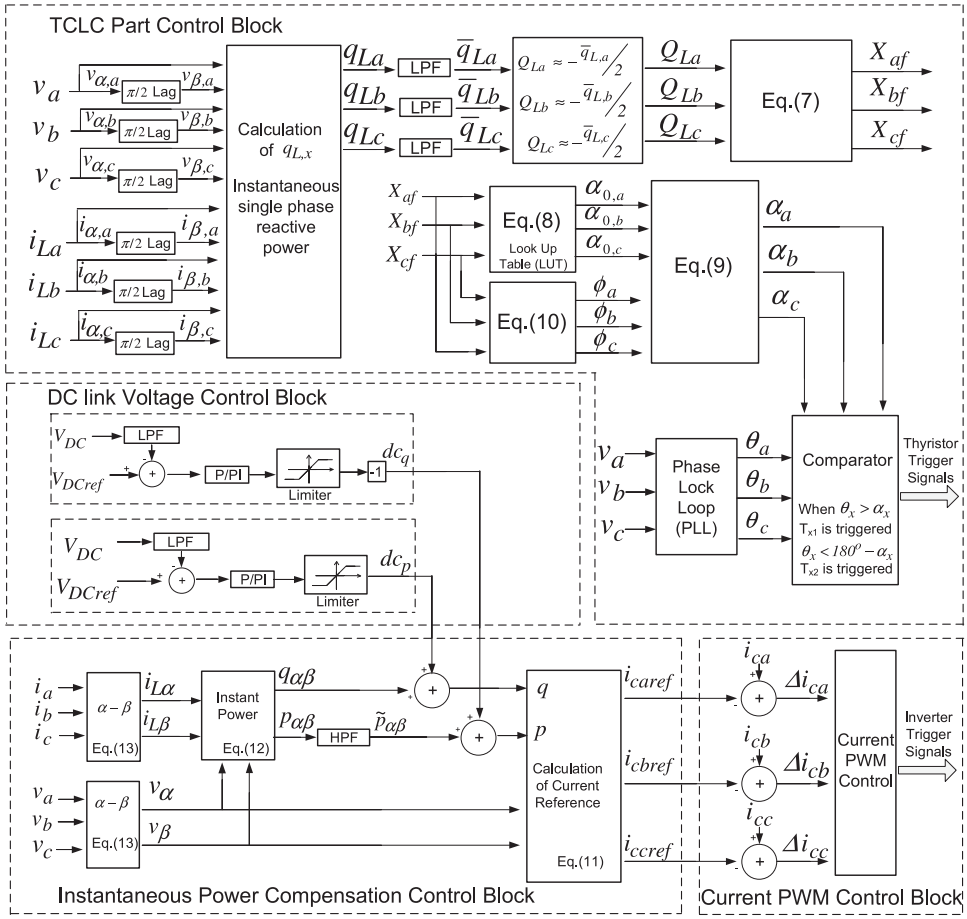

Fig. 4. Proposed hybrid control block diagram for the TCLC-HAPF under unbalanced loads compensation.

2) DC-Link Voltage Control: The active inverter part can effectively control the dc-link voltage by feeding back the dc-voltage-controlled signals which include both reactive and active components ($\mathrm{dc}_q, \mathrm{dc}_p$) [26] as shown in Fig. 4

$$\mathrm{dc}_q = -k_q \cdot (V_{\mathrm{DCref}} - V_{\mathrm{DC}}) \tag{14}$$

$$\mathrm{dc}_p = k_p \cdot (V_{\mathrm{DCref}} - V_{\mathrm{DC}}). \tag{15}$$

In (14) and (15), k_q and k_p are the proportional gains of the dc-link voltage controller. From [25]–[27], through the direct current hysteresis band PWM control, the dc voltage control reactive current component dc_q is used to step change the dc-link voltage during the start-up process, while the active current component dc_p is used to maintain the dc-link voltage as its reference due to the system loss, in which the dc-link voltage control with feedback both active dc_p and reactive dc_q component [25]–[27] can achieve both the start-up dc-link voltage self-charging function, maintaining the dc-link voltage and perform dynamic reactive power compensation simultaneously [25]–[27]. With the help of the three-phase instantaneous *pq* theory [5] and the terms of dc_q and dc_p, the dc-link voltage V_{DC} can track its reference V_{DCref} by transforming the dc voltage control signals into reference compensating currents through the above (11). Note that the dc-link control block requires a small amount of active power to maintain dc-link voltage at its reference value. The active power for maintaining dc-link voltage is taken equally from three phases, and it is relatively small comparing with the compensating one, so that it will not affect the unbalanced loading compensation of the TCLC part.

3) Current PWM Control: The final reference and actual compensating currents $i_{cx\mathrm{final}}$ and i_{cx} will be sent to the PWM control, and then PWM trigger signals for controlling the active inverter switching devices can be generated. The PWM method, such as triangular carrier-based sinusoid PWM or hysteresis PWM can be applied. In this paper, the hysteresis current PWM [29] is selected due to its advantages of fast response, ease of implementation, and good current limiting capability, etc.

C. Proposed Hybrid Controller for TCLC-HAPF

Based on the above discussions, the proposed hybrid control block diagram for the TCLC-HAPF under unbalanced loads compensation is shown in Fig. 4. It consists of five main control blocks: the TCLC part control block (discussed in Section III-A), the instantaneous power compensation control block (discussed in Section III-B1), the dc-link control block (discussed in Section III-B2), and the current PWM control block (discussed in Section III-B3).

In the following, simulation and experimental results of the proposed control strategy will be presented in comparison with

the state-of-the-art control strategy in [22] in order to verify its effectiveness and superior compensating performances under unbalanced loading condition.

IV. Simulation and Experimental Results

In this section, simulation and experimental results of the proposed TCLC-HAPF control strategy under unbalanced loading conditions will be presented and discussed in comparison with the results of the state-of-the-art control method in [22], in which the same dc-link voltage is applied to both of them. A 110-V 5-kVA three-phase three-wire TCLC-HAPF experimental prototype is designed and constructed in the laboratory. The details of the TCLC-HAPF experimental setup and its testing environment are provided in *Appendix C*. The simulations are carried out by using PSCAD/EMTDC, and the system parameters used in simulations are the same as the experiments as shown in Table V of *Appendix C*. In addition, with reference to the IEEE standard 519-2014 [31], the acceptable total demand distortion (TDD) $\leq 15\%$ with I_{SC}/I_L is in $100 < 1000$ scale (a small rating 110-V 5-kVA experimental prototype). The nominal rate current is assumed to be equal to the fundamental load current at the worst case analysis, which results in THD = TDD $\leq 15\%$. Therefore, this paper evaluates the TCLC-HAPF current harmonics compensating performance by setting an acceptable THD $\leq 15\%$.

Figs. 5 and 6 (simulation results) and Figs. 7 and 8 (experimental results) illustrate the waveforms of source currents, load currents (in Figs. 5, 6), compensating currents, capacitor (C_{PF}) currents, inductor (L_{PF}) currents, and dc-link voltage, source reactive and active power before and after compensation using the state-of-the-art control method [22] and the proposed control method. Figs. 9 and 10 (simulation results) and Figs. 11 and 12 (experimental results) and Table IV demonstrate the source current spectrums and phasor diagrams of source voltages and currents before and after the state-of-the-art control method [22] and the proposed control method. For each harmonic order of the current spectrum as in Fig. 11, the three bars from left to right represent phases *a*, *b*, and *c*, respectively. Moreover, Tables II–IV summarize all the simulation and experimental results shown in the aforementioned figures.

By using the control method in [22], the simulated and experimental system source PFs have been compensated to 0.93 and 0.95 (showing worst phase), respectively, as shown in Figs. 5 and 7, and Tables II and III. From Figs. 5(b), (c) and 7(b), (c), the source reactive power is compensated to 160 var, 9 var, and 237 var in the simulations and 130 var, 70 var, and 120 var in the experiments. Besides, the simulated source active power (483, 662, and 698 W) and experimental source active power (510, 680, and 690 W) are not balanced after compensations. Moreover, from Figs. 9(b) and 11(b) and Tables II and III, the simulated and experimental source current THD are compensated to 22.5% and 18.9% (showing worst phase), respectively. From Figs. 10(b) and 12(b), it can be seen that source voltage and current are not in phase (especially for phases *a* and *c*). In addition, as shown in Tables II and III, the simulated and experimental source current unbalanced factor (UBI_{fS}) is

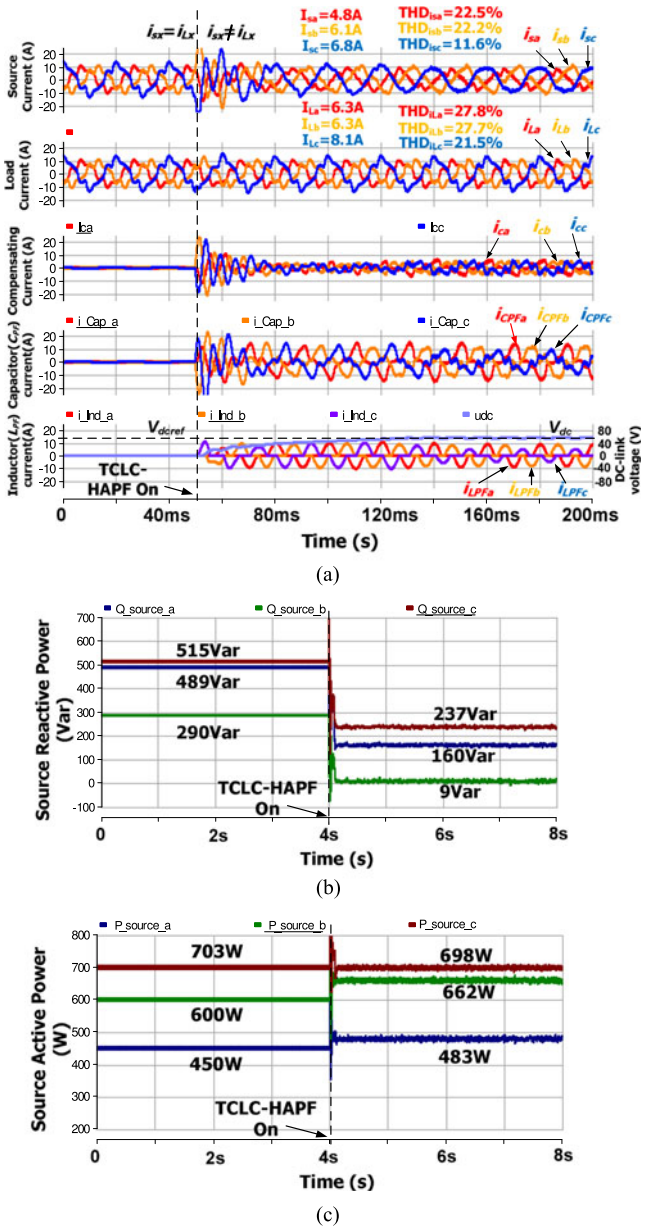

Fig. 5. Simulation results of dynamic performance by using the state-of-the-art control method [22] before and after compensation: (a) Source currents (i_{sx}), load currents (i_{Lx}), compensating currents (i_{cx}), capacitor (C_{PF}) currents, inductor (L_{PF}) currents, and dc-link voltage ($V_{\rm DC}$), (b) source reactive power Q_{sx}, and (c) source active power P_{sx}.

33.9% and 32.4%, respectively, after compensation. From Figs. 5 and 7, Figs. 9–12, Tables II–IV, it is proved that the state-of-the-art control method [22] cannot balance the source currents and provide good compensation performances with the small rating active inverter part under unbalanced loading condition.

By applying the proposed control method, the simulated and experimental system source PFs have been compensated to 0.99 or above in both the simulations and the experiments, as shown in Figs. 6 and 8, and Tables II and III. Figs. 6(b), (c) and 8(b), (c) illustrate that the three-phase simulated and experimental source reactive power have been compensated to close to zero and the source active power is approximately balanced after

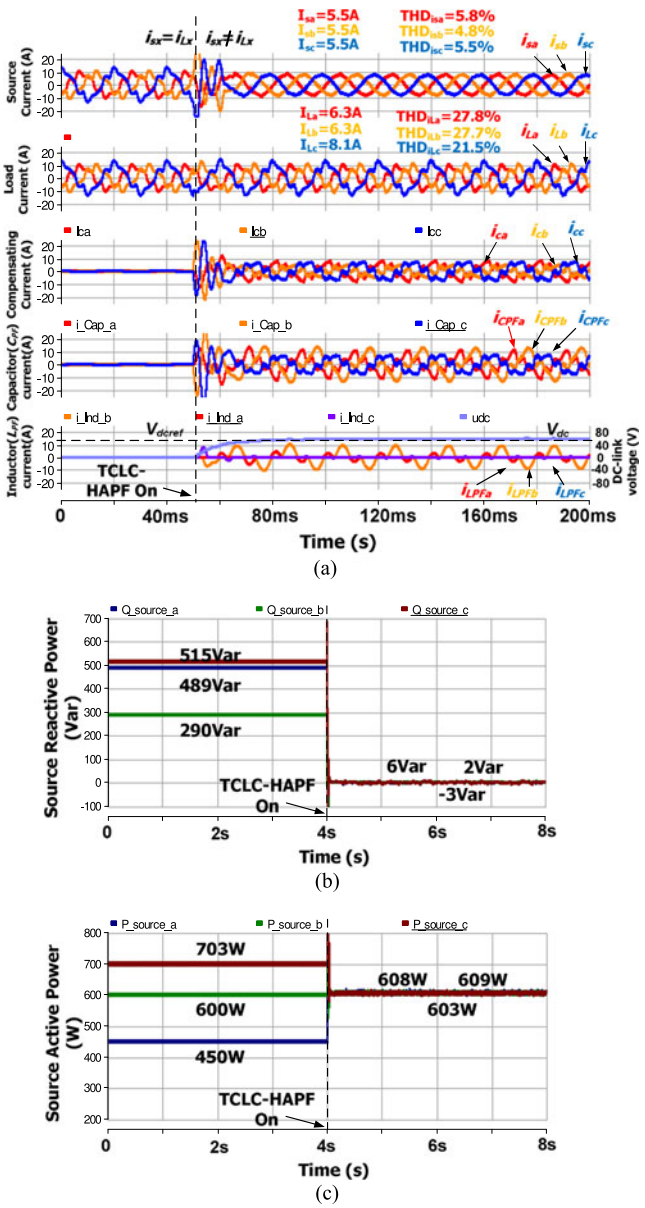

Fig. 6. Simulation results of dynamic performance by using the proposed control method before and after compensation: (a) Source currents (i_{sx}), load currents (i_{Lx}), compensating currents (i_{cx}), capacitor (C_{PF}) currents, inductor (L_{PF}) currents, and dc-link voltage ($V_{\rm DC}$), (b) source reactive power Q_{sx}, and (c) source active power P_{sx}.

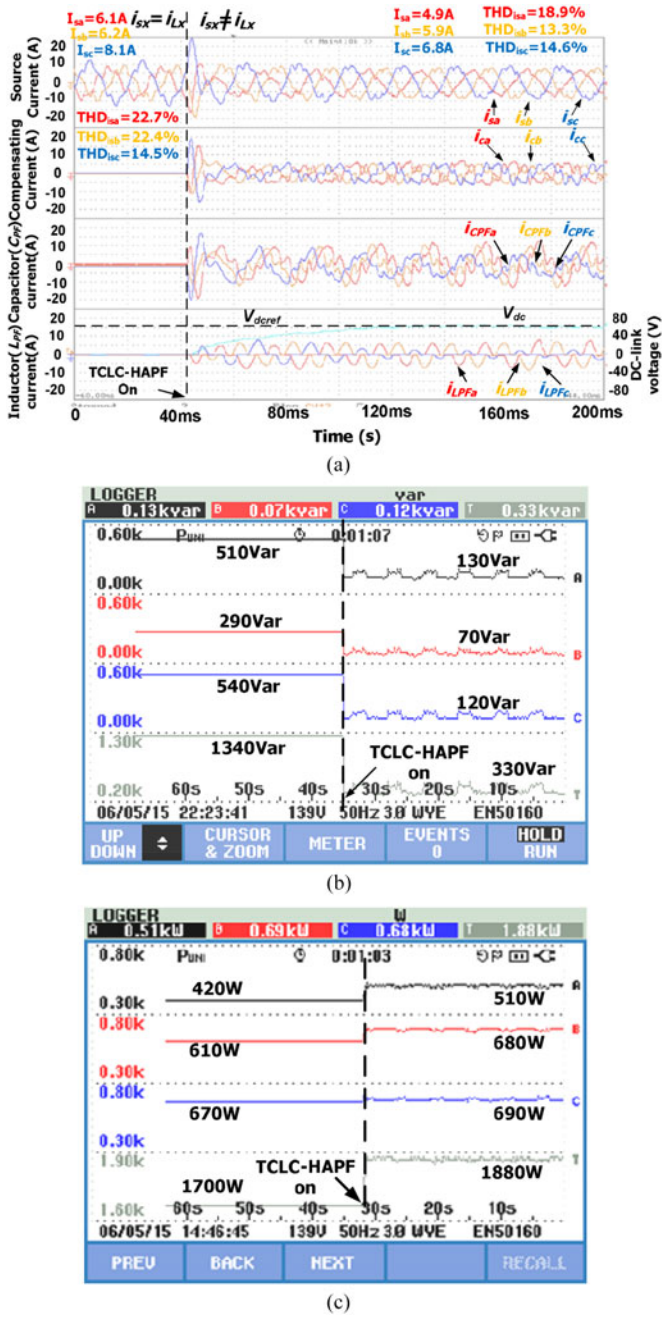

Fig. 7. Experimental results of dynamic performance by using the state-of-the-art control method [22] before and after compensation: (a) Source currents (i_{sx}), compensating currents (i_{cx}), capacitor (C_{PF}) currents, inductor (L_{PF}) currents, and dc-link voltage ($V_{\rm DC}$), (b) source reactive power Q_{sx}, and (c) source active power P_{sx}.

compensation. Moreover, from Figs. 9(c) and 11(c) and Tables II and III, the simulated and experimental source current THD have been compensated to 5.5% and 10.5% (showing worst phase), respectively. From Figs. 10(c) and 12(c), it can be seen that source voltage and current are in phase for all three phases. In addition, as shown in Tables II and III, the simulated and experimental source current unbalance factor (UBI_{fS}) is significantly reduced to 0.1% and 3.6% (from 26.0% and 29.4%) after compensation. From Figs. 5 and 7, Figs. 9–12, and Tables II–IV, they prove that the proposed method can simultaneously and effectively balance the source currents and provide satisfactory reactive power and current harmonics compensation performances with a small rating active inverter part under unbalanced loading condition.

In addition, the simulation results as shown in Figs. 5 and 6, Figs. 9 and 10, and Table II are consistent with experimental results shown in Figs. 7 and 8, Figs. 11 and 12, and Table III, which clearly verify the effectiveness and viability of the proposed unbalanced control strategy in comparison with the state-of-the-art one [22] for unbalanced loading compensation.

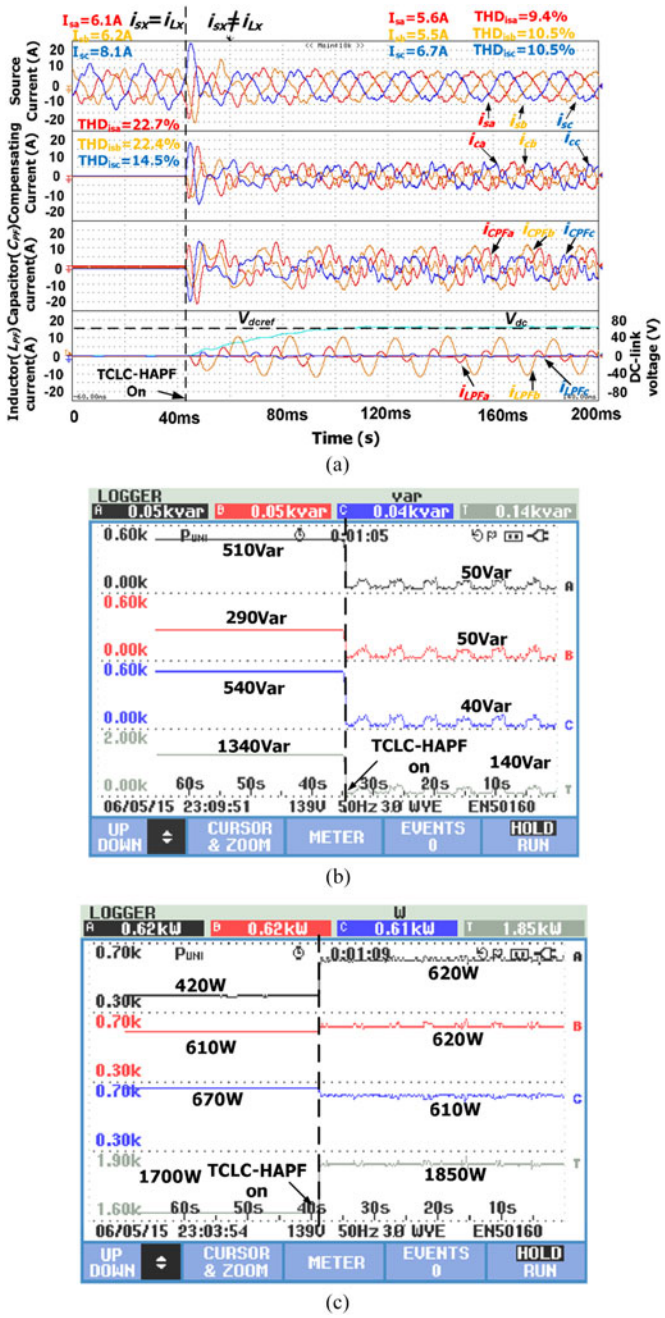

Fig. 8. Experimental results of dynamic performance by using the proposed control method before and after compensation: (a) Source currents (i_{sx}), load currents (i_{Lx}), compensating currents (i_{cx}), capacitor (C_{PF}) currents, inductor (L_{PF}) currents, and dc-link voltage (V_{DC}), (b) source reactive power Q_{sx}, and (c) source active power P_{sx}.

V. Conclusion

In this paper, a novel control strategy for a three-phase three-wire TCLC-HAPF is proposed, which can maintain it operating with a small rating active inverter part and at the same time it can balance the active power and compensate the reactive power and harmonic currents under unbalanced loading compensation. The design idea and operation steps of the proposed hybrid controller for the TCLC-HAPF under unbalanced loading is presented and discussed in details. Finally, simulation and experimental results are given to verify the proposed control method in comparison with the state-of-the-art control method, which shows its superior compensating performances under the unbalanced loading condition.

TABLE II
Simulation Results Before and After TCLC-HAPF Compensation by Using the State-of-the-Art Control Method [22] and the Proposed Method

		Q_{sx} (Var)	P_{sx} (W)	PF	i_{sxf} (A)	THD_{isx} (%)	UBI_{fS} (%)	V_{DC} (V)
Before Comp.	A	489	450	0.68	6.3	27.8	26.0	–
	B	290	600	0.90	6.3	27.7		
	C	515	703	0.80	8.1	21.5		
Control Method [22]	A	160	483	0.94	4.8	22.5	33.9	60
	B	9	662	0.99	6.1	22.2		
	C	237	698	0.94	6.8	11.6		
Proposed Method	A	6	608	0.99	5.5	5.2	0.1	60
	B	2	603	0.99	5.5	4.8		
	C	−5	609	0.99	5.5	5.5		

TABLE III
Experimental Results Before and After TCLC-HAPF Compensation by Using the State-of-the-Art Control Method [22] and the Proposed Method

		Q_{sx} (Var)	P_{sx} (W)	PF	i_{sxf} (A)	THD_{isx} (%)	UBI_{fS} (%)	V_{DC} (V)
Before Comp.	A	510	420	0.63	6.1	22.7	29.4	–
	B	290	610	0.89	6.2	22.4		
	C	540	670	0.78	8.1	14.5		
Control Method [22]	A	130	510	0.95	4.9	18.9	32.4	60
	B	70	680	0.98	5.9	13.3		
	C	120	690	0.97	6.8	14.6		
Proposed Method	A	50	620	0.99	5.6	9.4	3.6	60
	B	50	610	0.99	5.5	10.5		
	C	40	610	0.99	5.7	10.5		

Appendix

A. Balancing Three-Phase Fundamental Active Power by Reactive Power Compensation

In this appendix, the mathematical analysis is provided to show how the active power can be controlled to be balanced when the reactive power is compensated. Fig. 13 shows the power flow analysis before TCLC-HAPF compensation.

The phase fundamental apparent power is defined as $S_{sx} = P_{sx} + jQ_{sx} = \vec{V}_{sx} \cdot \vec{I}^{*}_{sxf}$ where the note "$*$" denotes the complex conjugate. In Fig. 13, the sum of $\vec{I}^{*}_{sxf}$ can be expressed as [30]:

$$\vec{I}^{*}_{saf} + \vec{I}^{*}_{sbf} + \vec{I}^{*}_{scf} = \frac{P_{sa} + jQ_{sa}}{\vec{V}_{saf}} + \frac{P_{sb} + jQ_{sb}}{\vec{V}_{sbf}} + \frac{P_{sc} + jQ_{sc}}{\vec{V}_{scf}} = 0 \tag{16}$$

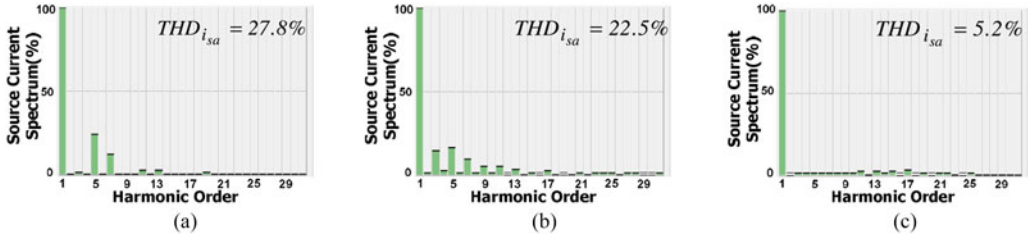

Fig. 9. Simulated source current spectrums of phase *a*: (a) Before compensation, (b) after state-of-the-art control method compensation [22], and (c) after the proposed control method compensation.

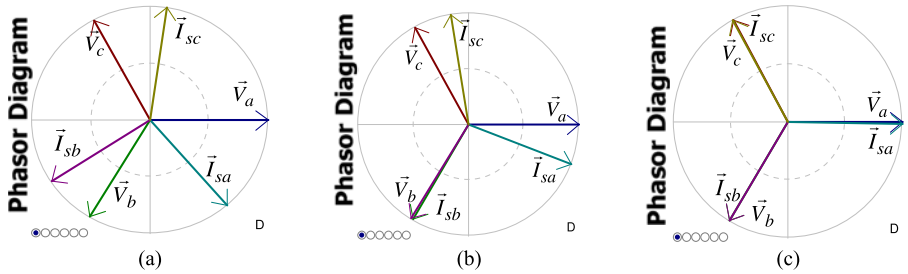

Fig. 10. Simulated phasor diagrams of source voltages and currents: (a) Before compensation, (b) after the state-of-the-art control method compensation [22], and (c) after the proposed control method compensation.

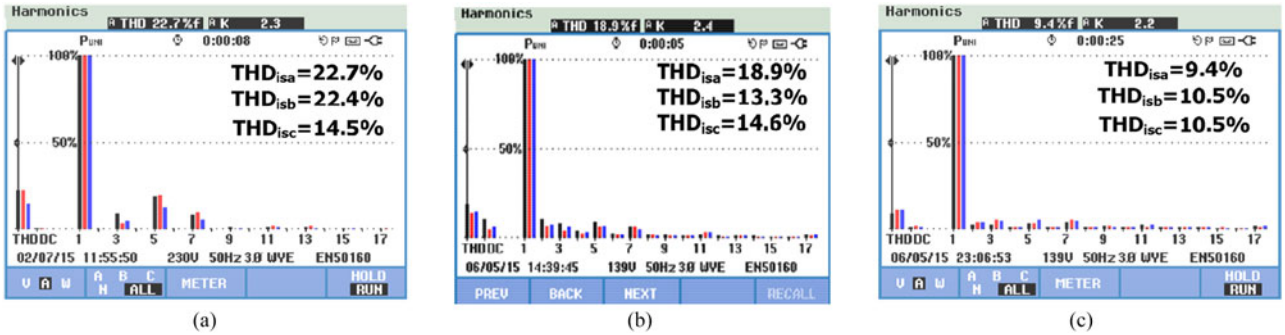

Fig. 11. Experimental source current spectrums: (a) Before compensation, (b) after the state-of-the-art control method compensation[22], and (c) after the proposed control method compensation.

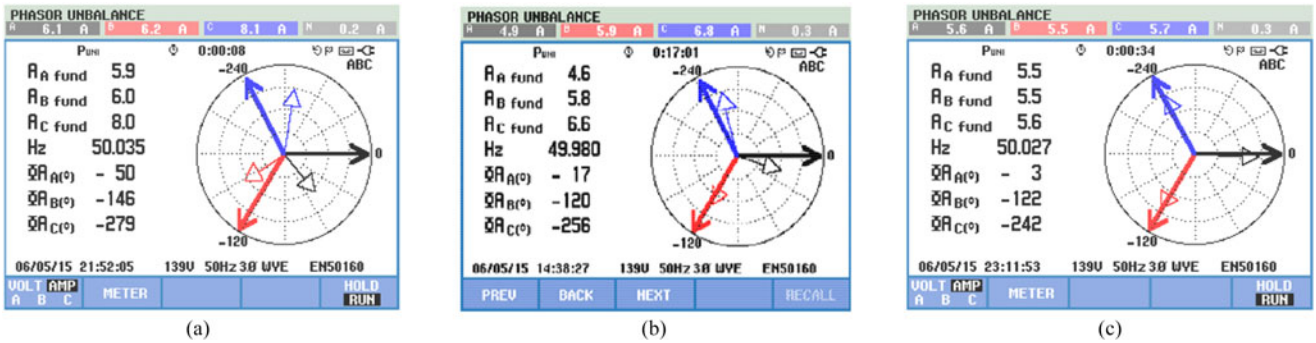

Fig. 12. Experimental phasor diagrams of source voltages and currents: (a) Before compensation, (b) after the state-of-the-art control method compensation [22], and (c) after the proposed control method compensation.

where $\vec{I}_{saf}$, $\vec{I}_{sbf}$, and $\vec{I}_{scf}$ are the fundamental source current phasors. $\vec{V}_{saf}$, $\vec{V}_{sbf}$, and $\vec{V}_{scf}$ are the fundamental load voltage phasors. $\vec{V}_{saf}$ is set to be the reference phasor, so $\vec{V}_{saf} = \bar{V}_{xf}\angle 0°$, $\vec{V}_{sbf} = \bar{V}_{xf}\angle -120°$, and $\vec{V}_{scf} = \bar{V}_{xf}\angle 120°$, where $1\angle -120° = -1/2 - j\sqrt{3}/2$ and $1\angle 120° = -1/2 + j\sqrt{3}/2$, $\bar{V}_{xf}$ is the rms value of the source voltage. Simplifying (16), one can get

$$\left(2P_{sa} - P_{sb} - \sqrt{3}Q_{sb} - P_{sc} + \sqrt{3}Q_{sc}\right) + j\left(2Q_{sa} - Q_{sb} + \sqrt{3}P_{sb} - Q_{sc} - \sqrt{3}P_{sc}\right) = 0. \quad (17)$$

TABLE IV
EXPERIMENTAL HARMONIC CURRENT VALUE OF EACH HARMONIC ORDER: BEFORE COMPENSATION, AFTER THE STATE-OF-THE-ART CONTROL METHOD COMPENSATION [22], AND AFTER THE PROPOSED CONTROL METHOD COMPENSATION

	Before Compensation						After control method [22] compensation						After proposed method compensation					
	Phase *a*		Phase *b*		Phase *c*		Phase *a*		Phase *b*		Phase *c*		Phase *a*		Phase *b*		Phase *c*	
Harmonic Order	(%)	(A)	(%)	(A)	(%)	(A)	(%)	(A)	(%)	(A)	(%)	(A)	(%)	(A)	(%)	(A)	(%)	(A)
1	100	5.1	100	4.9	100	7.4	100	3.8	100	5.2	100	5.7	100	4.6	100	4.6	100	4.8
2	0.1	0.01	0.1	0.00	0.1	0.01	10.1	0.38	7.3	0.38	8.4	0.48	3.4	0.16	4.1	0.19	4.1	0.20
3	9.5	0.48	4.1	0.20	6.4	0.47	8.9	0.34	3.6	0.19	6.1	0.35	3.6	0.17	4.9	0.23	4.3	0.21
4	0.2	0.01	0.1	0.00	0.1	0.01	5.1	0.19	2.5	0.13	2.5	0.14	0.8	0.04	0.3	0.01	0.5	0.02
5	18.2	0.93	20.2	0.99	12.1	0.90	8.4	0.32	7.1	0.37	7.9	0.45	4.0	0.18	3.7	0.17	4.9	0.24
6	0.1	0.01	0.1	0.00	0.2	0.01	2.1	0.08	0.4	0.02	0.5	0.03	0.3	0.01	0.3	0.01	0.3	0.01
7	6.8	0.35	7.3	0.36	3.3	0.24	6.5	0.25	6.5	0.34	3.9	0.22	4.6	0.21	5.8	0.27	4.7	0.23
8	0.2	0.01	0.2	0.01	0.1	0.01	1.3	0.05	0.2	0.01	0.4	0.02	0.2	0.01	0.2	0.01	0.2	0.01
9	2.0	0.10	0.8	0.04	0.3	0.02	1.2	0.05	0.2	0.01	0.6	0.03	0.3	0.01	1.0	0.05	0.2	0.01
10	0.2	0.01	0.1	0.00	0.2	0.01	0.3	0.01	0.3	0.02	0.3	0.02	1.2	0.06	0.7	0.03	0.7	0.03
11	2.7	0.14	2.2	0.11	1.1	0.08	1.7	0.06	2.3	0.12	2.4	0.14	2.6	0.12	1.6	0.07	2.6	0.12
12	0.1	0.01	0.2	0.01	0.1	0.01	0.8	0.03	0.1	0.01	0.3	0.02	0.6	0.03	1.6	0.07	1.8	0.09
13	2.8	0.14	2.3	0.11	0.2	0.03	1.2	0.05	0.4	0.02	0.9	0.05	2.8	0.13	1.6	0.07	1.6	0.08
14	0.1	0.01	0.1	0.00	0.1	0.01	0.5	0.02	0.1	0.01	0.3	0.02	1.2	0.06	1.2	0.06	1.2	0.06
15	0.8	0.04	0.3	0.01	0.1	0.02	0.4	0.02	0.2	0.01	0.1	0.01	1.3	0.06	1.3	0.06	1.3	0.06
16	0.2	0.01	0.1	0.00	0.2	0.01	0.1	0.01	0.1	0.01	0.1	0.01	1.3	0.06	1.3	0.06	1.3	0.06
17	0.7	0.04	0.7	0.03	0.1	0.02	1.5	0.06	0.7	0.04	0.9	0.05	1.8	0.08	1.3	0.06	1.8	0.09
THD	22.7	1.16	22.4	1.09	14.5	1.05	18.9	0.7	13.3	0.68	14.6	0.81	9.4	0.43	10.5	0.47	10.5	0.49

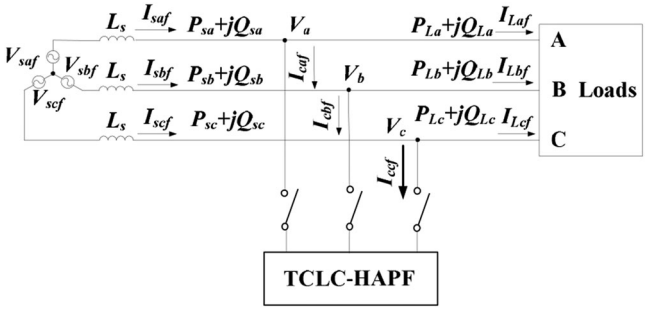

Fig. 13. Power flow analysis before compensation.

In (17), both real part and imaginary part needs to be zero. Thus

$$\begin{aligned} &2P_{sa} - P_{sb} - \sqrt{3}Q_{sb} - P_{sc} + \sqrt{3}Q_{sc} = 0 \\ &2Q_{sa} - Q_{sb} + \sqrt{3}P_{sb} - Q_{sc} - \sqrt{3}P_{sc} = 0. \end{aligned} \tag{18}$$

If the source reactive power is compensated to be zero by the TCLC-HAPF as

$$Q_{sa} = Q_{sb} = Q_{sc} = 0. \tag{19}$$

By substituting (19) into (18), the relationship of the three-phase source active power can be obtained as

$$P_{sa} = P_{sb} = P_{sc}. \tag{20}$$

Based on the analysis of (16)–(20), it can be concluded that the source active power can become balanced once the reactive power is compensated by the TCLC-HAPF. This idea can also be verified by the case study provided in the *Appendix B*.

B. Case Study of Section III-A

In this case study, referring to Fig. 2(b), the rms value of load voltage is given as $\bar{V}_x = 110\,\text{V}$, where $\vec{V}_a = \bar{V}_x \angle 0°$, $\vec{V}_b = \bar{V}_x \angle -120°$, and $\vec{V}_c = \bar{V}_x \angle 120°$, and the unbalanced phase load apparent power is assumed to be

$$\begin{bmatrix} P_{La} + jQ_{La} \\ P_{Lb} + jQ_{Lb} \\ P_{Lc} + jQ_{Lc} \end{bmatrix} = \begin{bmatrix} 233 + j438 \\ 363 + j203 \\ 498 + j429 \end{bmatrix}. \tag{21}$$

From (7) and (21), the required TCLC impedances for compensating the above unbalanced loading can be obtained as

$$\begin{bmatrix} X_{af} \\ X_{bf} \\ X_{cf} \end{bmatrix} = \begin{bmatrix} \frac{3\cdot\bar{V}_x^2\cdot(Q_{Lc}-Q_{Lb}-Q_{La})^{-1}\cdot(Q_{Lb}-Q_{La}-Q_{Lc})^{-1}}{(Q_{Lc}-Q_{Lb}-Q_{La})^{-1}+(Q_{La}-Q_{Lb}-Q_{Lc})^{-1}+(Q_{Lb}-Q_{La}-Q_{Lc})^{-1}} \\ \frac{3\cdot\bar{V}_x^2\cdot(Q_{Lc}-Q_{Lb}-Q_{La})^{-1}\cdot(Q_{La}-Q_{Lb}-Q_{Lc})^{-1}}{(Q_{Lc}-Q_{Lb}-Q_{La})^{-1}+(Q_{La}-Q_{Lb}-Q_{Lc})^{-1}+(Q_{Lb}-Q_{La}-Q_{Lc})^{-1}} \\ \frac{3\cdot\bar{V}_x^2\cdot(Q_{La}-Q_{Lb}-Q_{Lc})^{-1}\cdot(Q_{Lb}-Q_{La}-Q_{Lc})^{-1}}{(Q_{Lc}-Q_{Lb}-Q_{La})^{-1}+(Q_{La}-Q_{Lb}-Q_{Lc})^{-1}+(Q_{Lb}-Q_{La}-Q_{Lc})^{-1}} \end{bmatrix} = \begin{bmatrix} -22.75 \\ -77.58 \\ -24.62 \end{bmatrix}. \tag{22}$$

With the obtained TCLC impedances above, the final firing angles can be found through (8)–(10) as

$$\begin{bmatrix} \alpha_a \\ \alpha_b \\ \alpha_c \end{bmatrix} = \begin{bmatrix} \alpha_{0,a} \\ \alpha_{0,b} \\ \alpha_{0,c} \end{bmatrix} - \begin{bmatrix} \phi_a \\ \phi_b \\ \phi_c \end{bmatrix} = \begin{bmatrix} 145.4° \\ 122.3° \\ 141.8° \end{bmatrix} - \begin{bmatrix} -16.6° \\ -1.7° \\ 17.6° \end{bmatrix}$$

$$= \begin{bmatrix} 162.0^\circ \\ 124.0^\circ \\ 124.2^\circ \end{bmatrix}. \quad (23)$$

Then the corresponding source active power P_{sx} and reactive power Q_{sx} after TCLC compensation can be calculated by using the above X_{af}, X_{bf}, and X_{cf} values or simulated by using α_a, α_b, and α_c, which will be discussed in the following. If the conditions $P_{sa} = P_{sb} = P_{sc}$ and $Q_{sa} = Q_{sb} = Q_{sc} = 0$ are satisfied, it means that TCLC part can balance the active power and compensate reactive power of the unbalanced loading in (21). Thus, the validity of the proposed method can be verified.

With the required TCLC impedances in (22), load voltages $\vec{V}_x$ and the help of (3), the compensating currents $\vec{I}_{cxf}$ can be calculated as

$$\begin{bmatrix} \vec{I}_{caf} \\ \vec{I}_{cbf} \\ \vec{I}_{ccf} \end{bmatrix} = \begin{bmatrix} -j\left(\frac{X_b+X_c}{m}\right) & j\frac{X_{cf}}{m} & j\frac{X_{bf}}{m} \\ j\frac{X_{cf}}{m} & -j\left(\frac{X_{af}+X_{cf}}{m}\right) & j\frac{X_{af}}{m} \\ j\frac{X_b}{m} & j\frac{X_{af}}{m} & -j\left(\frac{X_{af}+X_{bf}}{m}\right) \end{bmatrix} \cdot \begin{bmatrix} \vec{V}_a \\ \vec{V}_b \\ \vec{V}_c \end{bmatrix} = \begin{bmatrix} 4.16\angle 72.98^\circ \\ 1.88\angle -30.72^\circ \\ 4.14\angle -133.35^\circ \end{bmatrix}, \quad (24)$$

where

$$\begin{bmatrix} X_a/m \\ X_b/m \\ X_c/m \end{bmatrix} = \begin{bmatrix} \frac{X_{af}}{X_{af}X_{bf}+X_{bf}X_{cf}+X_{cf}X_{af}} \\ \frac{X_{bf}}{X_{af}X_{bf}+X_{bf}X_{cf}+X_{cf}X_{af}} \\ \frac{X_{cf}}{X_{af}X_{bf}+X_{bf}X_{cf}+X_{cf}X_{af}} \end{bmatrix} = \begin{bmatrix} 5.37\times 10^{-3} \\ 18.32\times 10^{-3} \\ 5.81\times 10^{-3} \end{bmatrix}.$$

The phase load currents $\vec{I}_{Lxf}$ can be calculated as

$$\begin{bmatrix} \vec{I}_{Laf} \\ \vec{I}_{Lbf} \\ \vec{I}_{Lcf} \end{bmatrix} = \begin{bmatrix} \left[(P_{La}+jQ_{La})/\vec{V}_a\right]^* \\ \left[(P_{Lb}+jQ_{Lb})/\vec{V}_b\right]^* \\ \left[(P_{Lc}+jQ_{Lc})/\vec{V}_c\right]^* \end{bmatrix} = \begin{bmatrix} 4.51\angle -61.93^\circ \\ 3.76\angle -149.50^\circ \\ 5.99\angle 79.14^\circ \end{bmatrix}. \quad (25)$$

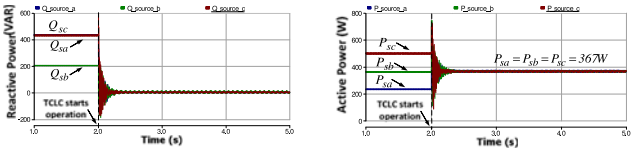

Fig. 14. Simulated source reactive power Q_{sx} and active power P_{sx} before and after TCLC compensation: (a) Q_{sx} and (b) P_{sx}.

From (24) and (25), the source currents after TCLC compensation can be calculated as

$$\begin{bmatrix} \vec{I}_{saf} \\ \vec{I}_{sbf} \\ \vec{I}_{scf} \end{bmatrix} = \begin{bmatrix} \vec{I}_{Laf} \\ \vec{I}_{Lbf} \\ \vec{I}_{Lcf} \end{bmatrix} + \begin{bmatrix} \vec{I}_{caf} \\ \vec{I}_{cbf} \\ \vec{I}_{ccf} \end{bmatrix} = \begin{bmatrix} 3.34\angle 0^\circ \\ 3.34\angle -120^\circ \\ 3.34\angle 120^\circ \end{bmatrix}. \quad (26)$$

Moreover, the active power and reactive power at source side can be calculated as

$$\begin{bmatrix} P_{sa}+jQ_{sa} \\ P_{sb}+jQ_{sb} \\ P_{sc}+jQ_{sc} \end{bmatrix} = \begin{bmatrix} \vec{V}_a\vec{I}^*_{saf} \\ \vec{V}_b\vec{I}^*_{sbf} \\ \vec{V}_c\vec{I}^*_{scf} \end{bmatrix} = \begin{bmatrix} 367+j0 \\ 367+j0 \\ 367+j0 \end{bmatrix}. \quad (27)$$

In (27), as $P_{sa} = P_{sb} = P_{sc}$ and $Q_{sa} = Q_{sb} = Q_{sc} = 0$, it can be clearly shown that the calculated TCLC impedances in (22) can balance and compensate the active and reactive power. Moreover, under unbalanced loading as shown in (21), Fig. 14 shows the simulated Q_{sx} and P_{sx} before and after compensation by applying the proposed TCLC control method with the firing angles α_x obtained in (23). In Fig. 14, Q_{sx} have been compensated to zero while P_{sx} are balanced after the TCLC compensation. Besides, the simulation results are consistent with the theoretical results. Therefore, from the results shown in (27) and Fig. 14 of the case study, it can be verified that the proposed TCLC control method can balance active power and compensate reactive power.

C. Experimental Setup for a 110-V 5-kVA Three-Phase Three-Wire TCLC-HAPF Experimental Prototype

An 110-V 5-kVA three-phase three-wire TCLC-HAPF experimental prototype is designed and constructed in the laboratory and the testing environment is shown in Fig. 15. The digital control system of the TCLC-HAPF consists of two paralleled digital signal processors (DSPs) TMS320F2812s, and the basic settings of both DSPs are the same. The sampling frequency of the control system is 25 kHz in both simulation and experiment (for both DSPs). For every 1/25 kHz(s) period, the timer will provide a signal to process analog to digital (A/D) conversion and the corresponding interrupt. After processing the proposed control strategy, the output PWMs signal will be generated and the maximum PWM switching frequency is 12.5 kHz. The SanRex PK110FG160 thyristors are used for the TCLC part, while the Mitsubishi IGBT intelligent power modules PM300DSA60 are employed as the switching devices of the inverter. To capture the experimental results, the voltage and current waveforms are measured by an oscilloscope "Yokogawa DL750" and

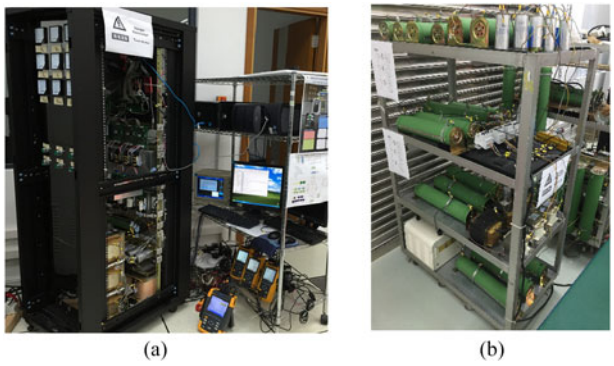

(a) (b)

Fig. 15. Experimental setup: (a) 110-V 5-kVA TCLC-HAPF experimental prototype and its testing environment and (b) testing loads.

TABLE V
TCLC-HAPF EXPERIMENTAL PARAMETERS FOR POWER QUALITY COMPENSATION

	Parameters	Physical values
System parameters	v_x, f	110 V, 50 Hz
TCLC-HAPF parameters	L_c, L_{PF}, C_{PF}	5 mH(Q = 18, ESR = 0.09 Ω)
		30 mH(Q = 23, ESR = 0.41 Ω)
		160 μF(Q = 310, ESR = 0.06 Ω)
	$C_{\mathrm{DC}}, V_{\mathrm{DC}}$	5 mF, 60 V
	Q_{cx} range	[−630 var, 600 var]

Notes: Q stands for the quality factor and ESR stands for equivalent series resistance.

the current harmonic spectrums for three phase are measured by a power quality analyzer "Fluke 435." The system and TCLC-HAPF parameters for experiments are summarized in Table V, and the photograph of TCLC-HAPF experimental prototype with its testing environment and testing loads is shown in Fig. 15.

The compensating reactive power Q_{cx} range in term of TCLC impedance $X_{\mathrm{TCLC}}(\alpha_x)$ or firing angle α_x can be expressed as

$$Q_{cx}(\alpha_x) = \frac{\bar{V}_x^2}{X_{\mathrm{TCLC}}(\alpha_x)} = \frac{\bar{V}_x^2}{\frac{\pi X_{L_{PF}} X_{C_{PF}}}{X_{C_{PF}}[2\pi - 2\alpha_x + \sin(2\alpha_x)] - \pi X_{L_{PF}}} + X_{L_c}} \quad (28)$$

where $\bar{V}_x$ is the rms value of load voltage, X_{L_c}, $X_{L_{PF}}$, and $X_{C_{PF}}$ are the impedance of Lc, L_{PF}, and C_{PF}, respectively. When both thyristors are turned off for the whole fundamental period (firing angle $\alpha_x = 180°$), the TCLC part can be considered as an LC filter (L_c and C_{PF}). In this case, the TCLC is providing the maximum capacitive compensating reactive power $Q_{cx(\mathrm{MaxCap})}$. On the other hand, when one of the thyristors is turned on for half of a fundamental period alternately (firing angle $\alpha_x = 90°$), the TCLC part can be considered as the L_c in series with the parallel combination of L_{PF} and C_{PF}. At this case, the TCLC filter provides the maximum inductive compensating reactive power $Q_{cx(\mathrm{MaxInd})}$ as $\alpha_x = 90°$. With the system parameters as shown in Table V and (28), the compensating reactive power range can be plotted in Fig. 16.

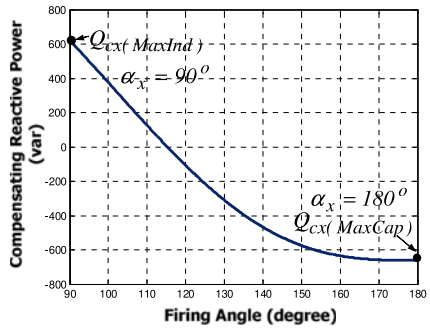

Fig. 16. Relationship between the firing angle and the compensating reactive power.

REFERENCES

[1] S. Y. Lee and C. J. Wu, "Reactive power compensation and load balancing for unbalanced three-phase four-wire system by a combined system of an SVC and a series active filter," *Proc. IEE Electr. Appl.*, vol. 147, no. 6, pp. 563–570, 2000.

[2] G. Gueth, P. Enstedt, A. Rey, and R. W. Menzies, "Individual phase control of a static compensator for load compensation and voltage balancing and regulation," *IEEE Trans. Power Syst.*, vol. 2, no. 4, pp. 898–905, Nov. 1987.

[3] G. Tang, K. Zha, Z. He, and H. Wang, "Study on operational tests for FACTS thyristor valves," *IEEE Trans. Power Del.*, vol. 28, no. 3, pp. 1525–1532, Jul. 2013.

[4] E. Ghahremani and I. Kamwa, "Analysing the effects of different types of FACTS devices on the steady-state performance of the Hydro-Québec network," *IET Gener. Transmiss. Distrib.*, vol. 8, no. 2, pp. 233–249, May 2013.

[5] H. Akagi, Y. Kanazawa, and A. Nabae, "Instantaneous reactive power compensators comprising switching devices without energy storage components," *IEEE Trans. Ind. Appl.*, vol. IA-20, no. 3, pp. 625–630, May 1984.

[6] H. Haibing and X. Yan, "Design considerations and fully digital implementation of 400-Hz active power filter for aircraft applications," *IEEE Trans. Ind. Electron.*, vol. 61, no. 8, pp. 3823–3834, Aug. 2014.

[7] Y. Hu, Z. Zhu, and K. Liu, "Current control for dual three-phase permanent magnet synchronous motors accounting for current unbalance and harmonics," *IEEE Trans. Emerg. Sel. Topics Power Electron.*, vol. 2, no. 2, pp. 272–284, Jun. 2014.

[8] M. Aredes, H. Akagi, E. H. Watanabe, E. Vergara Salgado, and L. F. Encarnacao, "Comparisons between the p–q and p–q–r theories in three-phase four-wire systems," *IEEE Trans. Power Electron.*, vol. 24, no. 4, pp. 924–933, Apr. 2009.

[9] B. Wen, D. Boroyevich, R. Burgos, P. Mattavelli, and Z. Shen, "Analysis of D-Q small-signal impedance of grid-tied inverters," *IEEE Trans. Power Electron.*, vol. 31, no. 1, pp. 675–687, Jan. 2016.

[10] L. Shaohua, W. Xiuli, Y. Zhiqing, L. Tai, and P. Zhong, "Circulating current suppressing strategy for MMC-HVDC based on nonideal proportional resonant controllers under unbalanced grid conditions," *IEEE Trans. Power Electron.*, vol. 30, no. 1, pp. 387–397, Jan. 2015.

[11] X. Guo, W. Liu, X. Zhang, X. Sun, Z. Lu, and J. M. Guerrero, "Flexible control strategy for grid-connected inverter under unbalanced grid faults without PLL," *IEEE Trans. Power Electron.*, vol. 30, no. 4, pp. 1773–1778, Apr. 2015.

[12] K. Ma, W. Chen, M. Liserre, and F. Blaabjerg, "Power controllability of a three-phase converter with an unbalanced AC source," *IEEE Trans. Power Electron.*, vol. 30, no. 3, pp. 1591–1604, Mar. 2015.

[13] M. Castilla, J. Miret, A. Camacho, L. Garcia de Vicuna, and J. Matas, "Modeling and design of voltage support control schemes for three-phase inverters operating under unbalanced grid conditions," *IEEE Trans. Power Electron.*, vol. 29, no. 11, pp. 6139–6150, Nov. 2014.

[14] S. Srianthumrong and H. Akagi, "A medium-voltage transformerless AC/DC Power conversion system consisting of a diode rectifier and a shunt hybrid filter," *IEEE Trans. Ind. Appl.*, vol. 39, no. 3, pp. 874–882, May/Jun. 2003.

[15] W. C. Lee, T. K. Lee, and D. S. Hyun, "A three-phase parallel active power filter operating with PCC voltage compensation with consideration for an unbalanced load," *IEEE Trans. Power Electron.*, vol. 17, no. 5, pp. 807–814, Sep. 2002.

[16] S. Senini and P. J. Wolfs, "Hybrid active filter for harmonically unbalanced three phase three wire railway traction loads," *IEEE Trans. Power Electron.*, vol. 15, no. 4, pp. 702–710, Jul. 2000.
[17] S. Rahmani, K. Al-Haddad, and F. Fnaiech, "A three phase shunt hybrid power filter adopted a general algorithm to compensate harmonics, reactive power and unbalanced load under nonideal mains voltages," in *Proc. IEEE Int. Conf. Ind. Technol.*, 2004, pp. 651–656.
[18] S. Rahmani, A. Hamadi, and K. Al-Haddad, "A lyapunov-function-based control for a three-phase shunt hybrid active filter," *IEEE Trans. Ind. Electron.*, vol. 59, no. 3, pp. 1418–1429, Mar. 2012.
[19] P. Salmeron and S. P. Litr, "A control strategy for hybrid power filter to compensate four-wires three-phase systems," *IEEE Trans. Power Electron.*, vol. 25, no. 7, pp. 1923–1931, Jul. 2010.
[20] L. S Czarnecki and S. E Pearce, "Compensation objectives and currents' physical components-based generation of reference signals for shunt switching compensator control," *IET Power Electron.*, vol. 2, no. 1, pp. 33–41, Jan. 2009.
[21] L. S Czarnecki and P. M, Haley, "Unbalanced power in four-wire systems and its reactive compensation," *IEEE Trans. Power Del.*, vol. 30, no. 1, pp. 53–63, Feb. 2015.
[22] S. Rahmani, A. Hamadi, and K. Al-Haddad, "A combination of shunt hybrid power filter and thyristor-controlled reactor for power quality," *IEEE Trans. Ind. Electron.*, vol. 61, no. 5, pp. 2152–2164, May 2014.
[23] C.-S. Lam, M.-C. Wong, and Y.-D. Han, "Voltage swell and overvoltage compensation with unidirectional power flow controlled dynamic voltage restorer," *IEEE Trans. Power Del.*, vol. 23, no. 4, pp. 2513–2521, Oct. 2008.
[24] C.-S. Lam, X.-X. Cui, W.-H Choi, M.-C. Wong, and Y.-D. Han, "Minimum inverter capacity design for three-phase four-wire LC-hybrid active power filters," *IET, Power Electron.*, vol. 5, no. 7, pp. 956–968, Aug. 2012.
[25] C.-S. Lam, W.-H. Choi, M.-C. Wong, and Y.-D. Han, "Adaptive dc-link voltage controlled hybrid active power filters for reactive power compensation," *IEEE Trans. Power Electron.*, vol. 27, no. 4, pp. 1758–1772, Apr. 2012.
[26] C.-S. Lam, M.-C. Wong, W.-H. Choi, X.-X. Cui, H.-M. Mei, and J.-Z. Liu, "Design and performance of an adaptive low-dc-voltage-controlled LC-Hybrid active power filter with a neutral inductor in three-phase four-wire power systems," *IEEE Trans. Ind. Electron.*, vol. 61, no. 6, pp. 2635–2647, Jun. 2014.
[27] W.-H. Choi, C.-S. Lam, M.-C. Wong, and Y.-D. Han, "Analysis of dc-link voltage controls in three-phase four-wire hybrid active power filters," *IEEE Trans. Power Electron.*, vol. 28, no. 5, pp. 2180–2191, May 2013.
[28] V. Khadkikar, A. Chandra, and B. N. Singh, "Generalized single-phase p-q theory for active power filtering: Simulation and DSP-based experimental investigation," *IET Power Electron*, vol. 2, pp. 67–78, Jan. 2009.
[29] C.-S. Lam, M.-C. Wong, and Y.-D. Han, "Hysteresis current control of hybrid active power filters," *IET Power Electron.*, vol. 5, no. 7, pp. 1175–1187, Aug. 2012.
[30] F. R. Quintela, J. M. G. Arevalo, and R. C. Redondo, "Power analysis of static var compensators," *Electr. Power Syst. Res.*, vol. 30, no. 6, pp. 376–382, 2008.
[31] *IEEE Recommended Practices and Requirements for Harmonic Control in Electrical Power Systems*, IEEE Standard 519-2014, 2014.

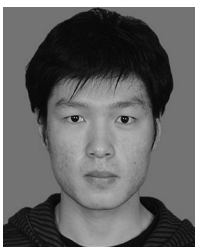

Lei Wang received the B.Sc. degree in electrical and electronics engineering from the University of Macau (UM), Macao, China, in 2011, and the M.Sc. degree in electronics engineering from the Hong Kong University of Science and Technology, Hong Kong, in 2012. Since 2012, he has been working toward the Ph.D. degree in electrical and computer engineering at the Power Electronics Laboratory, UM.

His research interests include power electronics, power quality and distribution flexible ac transmission system, power quality compensation, and renewable energy.

Mr. Wang received the champion award in the "Schneider Electric Energy Efficiency Cup," Hong Kong, in 2011.

Chi-Seng Lam (S'04–M'12–SM'16) received the B.Sc., M.Sc., and Ph.D. degrees in electrical and electronics engineering from the University of Macau (UM), Macao, China, in 2003, 2006, and 2012, respectively.

From 2006 to 2009, he was an E&M Engineer with UM. In 2009, he simultaneously worked as a Laboratory Technician and started to pursue his Ph.D. degree and completed within three years. In 2013, he was a Postdoctoral Fellow with The Hong Kong Polytechnic University, Hong Kong. He is currently an Assistant Professor at the State Key Laboratory of Analog and Mixed-Signal VLSI, UM. He has coauthored two books: "*Design and Control of Hybrid Active Power Filters"* (New York, NY, USA: Springer, 2014) and "*Parallel Power Electronics Filters in Three-phase Four-wire Systems—Principle, Control and Design"* (New York, NY, USA: Springer, in press), one U.S. patent, two Chinese patents, and more than 50 technical journals and conference papers. His research interests include integrated power electronics controllers, power management integrated circuits, power quality compensators, smart grid technology, renewable energy, etc.

Dr. Lam received the Macao Science and Technology Invention Award (Third-Class) and an R&D Award for Postgraduates (Ph.D.) in 2014 and 2012, respectively. He also received the Macao Government Ph.D. Research Scholarship in 2009–2012, the Macao Foundation Postgraduate Research Scholarship in 2003–2005, and the third RIUPEEEC Merit Paper Award in 2005. In 2007, 2008, and 2015, he was the Gold Officer, Student Branch Officer, and Secretary of the IEEE Macau Section. He is currently the Vice-Chair of the IEEE Macau Section and Secretary of the IEEE Macau PES/PELS Joint Chapter. He was the Local Arrangement Chair of TENCON 2015 and ASP-DAC 2016.

Man-Chung Wong (SM'06) received the B.Sc. and M.Sc. degrees in electrical and electronics engineering from the University of Macau (UM), Macao, China, in 1993 and 1997, respectively, and the Ph.D. degree in electrical engineering from Tsinghua University, Beijing, China, in 2003.

He was a Visiting Fellow with Cambridge University, U.K., in 2014. He is currently an Associate Professor at the Department of Electrical and Computer Engineering, UM. He has coauthored two Springer books, more than 100 journal and conference papers, and six patents (China and USA). His research interests include power electronics converters, pulse with modulation, active power filters, hybrid active power filters, and hybrid power quality compensator for high-speed railway power supply system. Recently, an industrial power filter platform was developed and installed in a practical power system based on his research results.

Prof. Wong received the Macao Young Scientific Award from the Macau International Research Institute in 2000, the Young Scholar Award of UM in 2001, the Second Prize for the Tsinghua University Excellent Ph.D. Thesis Award in 2003, and the Macao Science and Technology Invention Award (Third-Class) in 2012 and 2014, respectively. He supervised several students to receive merit paper awards in conferences and champions in student project competitions. He was several conference committee members and General Chair of the IEEE TENCON 2015 in Macau. In 2014–2015, he was an IEEE Macau Section Chair. Recently, he is a North Representative of the IEEE Region 10 Power and Energy Society and the IEEE Macau PES/PELS Joint Chapter Chair.